Nanoscale

Gel polymer electrolyte for Room temperature Sodium Sulfur batteries

Journal:	*Nanoscale*
Manuscript ID	NR-ART-03-2025-001049
Article Type:	Paper
Date Submitted by the Author:	11-Mar-2025

Complete List of Authors:	Nguyen, Hao; The University of New Mexico, Department of Chemical and Biological Engineering Li, Jiahan; The University of New Mexico, Department of Chemical and Biological Engineering Vadthya, Raju; The University of New Mexico, Department of Chemical and Biological Engineering Wei, Shuya; The University of New Mexico, Department of Chemical and Biological Engineering

Gel polymer electrolyte for Room temperature Sodium Sulfur batteries

Hao Nguyen[1], Jiahan Li[1], Raju Vadthya[1], and Shuya Wei[1*]

1. Department of Chemical and Biological Engineering, University of New Mexico, Albuquerque, New Mexico, United States.

Corresponding Author

Shuya Wei, swei@unm.edu

Abstract

Sodium sulfur batteries have gained attention owing to the advantages of low cost and high specific capacity. However, the current electrolytes have a few main disadvantages, including sodium-dendrite growth, sulfur shuttling and electrolyte leakage, which hinder their practical application. Herein, we report the preparation of poly(vinylidene fluoride-co-hexafluoropropylene) based gel polymer electrolytes by a simple solution casting technique for room temperature sodium sulfur battery applications. The gel polymer electrolyte was activated by soaking the freshly prepared gel polymer membranes in a liquid electrolyte solution. Our gel polymer electrolyte exhibits a high ionic conductivity of 1.37 mS cm^{-1} at ambient temperature with the electrochemical stability window of 4.5V versus Na^+/Na. Furthermore, sodium symmetric cells show stable stripping/plating of Na^+ up to 3000 hours with transference number of 0.648. The cells achieved a specific capacity of 398 mAh g^{-1} for the initial reversible discharge specific capacity and 75 mAh g^{-1} at cycle 200 with 99.9% Coulombic efficiency at 0.1C rate. Our results demonstrate the polymer electrolytes are a potential candidate for sodium sulfur batteries with desired performance.

Keywords

Sodium–sulfur batteries, separator, gel polymer electrolytes, solution casting

1. Introduction

Nowadays, lithium-ion batteries are widely used for daily life energy storage from small portable electronic devices to medium electric vehicles and large power grid.[1,2] However, lithium is scarce, and its cost is rising due to the ongoing surge in demand for this battery technology. In view of that, developing materials that offer high energy density, greater abundance, and lower production costs are of utmost importance. Therefore, sodium–sulfur batteries (NaSBs), which use inexpensive and environmentally benign materials of sodium and sulfur, have attracted substantial interest in recent years due to high specific capacity (1675 mAh g_{sulfur}^{-1}). Analogous to the components of a lithium-ion batteries cell, a NaSBs also comprises cathode, anode, separator and electrolyte. The major drawback of this conventional cell's configuration is the lack of safety due to flammable organic electrolytes in the system. Despite having high ionic conductivities (10^{-3} to 10^{-2} S cm^{-1}), conventional organic liquid electrolytes (LEs) present several significant issues. First, LEs can cause dendrite growth due to nonuniform currents distribution. The main concern of using ~~for~~ LEs arises from risks of leakage leading to fire hazards.[3–5] Moreover, LEs face significant disadvantages from polysulfide shuttling effect. Compared to LEs, polymer electrolytes (PEs) are profoundly favored for energy storage applications, since they can oblige volume changes of the electrodes amid electrochemical processes, encourage the adaptable designs of batteries with diverse shapes. Furthermore, the hindering effects such as leakage of electrolyte can be minimized by using polymer electrolytes.[6–9] However, solid polymer electrolytes are also having some drawbacks such as low electrical conductivity (10^{-8} to 10^{-5} S cm^{-1}) at room temperature and poor electrode/electrolyte interfaces.[10–13] Various approaches have been explored to develop PEs that exhibit enhanced conductivity at room temperature and maintain stable interfaces between electrodes and electrolytes. Researchers have focused on improving the ionic conductivity of PEs under ambient conditions while simultaneously ensuring robust interfacial properties to enhance overall battery performance.[14–17]

With the aim to overcome the issues mentioned above, the liquid electrolytes were incorporated in~~to~~ a solid polymer membrane to form gel polymer electrolytes (GPEs) which embraces both the characteristics of PEs and LEs.[14] The properties of polymer membrane essentially porosity, wettability, and tortuosity of the pores are greatly influenced by its processing methods. Distinctive techniques such as solution casting, phase inversion, UV curing, in situ polymerization and electrospinning method.[16,18–23] Among the available methods, solution casting stands out as the most straightforward yet modestly scalable approach. This technique involves blending the LEs with the polymer precursor, then spreading the mixture onto a glass surface and allowing it to dry in a vacuum chamber. Once the gel polymer electrolyte (GPE) membrane is freshly prepared, it is immersed in the same liquid electrolyte to absorb the solution and swell.

In GPEs, polyvinylidene fluoride (PVDF), poly vinylidene fluoride-co-hexafluoropropylene (PVDF-HFP), polyacrylonitrile (PAN), and polymethyl methacrylate (PMMA) have been widely used as polymer hosts. Among them, PVDF-HFP have received great attention because of their amorphous nature and its potentiality to display high room temperature ionic conductivity, and strong chemical resistance, high thermal stability and flexibility.[24–26] Also, PVDF-HFP based GPEs has a high dielectric constant of 8.4 and strong electron-withdrawing functional group (-C-

F), which advances to the greater disintegration of salts and subsequently supports a high concentration of charge carriers.[27] Kumar et al.[9] successfully fabricated GPE using PVDF-HFP backbone and SiO_2 as additive for NaSBs. Despite having high conductivity of 4.1 mS cm^{-1} and sodium ion transport number of 0.52, the batteries failed to run multiple cycles and only produced specific capacity of 165 mAh g^{-1} on the first discharge. Janakiraman et al.[25] reported the preparation of PVDF-HFP using a simple electrospinning technique and the GPE was activated by soaking in LE. The GPE has higher ionic conductivity of $1.13x10^{-3}$ S cm^{-1} than commercial separator Celgard 2400 with $0.36x10^{-4}$ S cm^{-1}. However, there are many draw back using electrospinning technique such as low commercial impact and scalability for large-scale application due to limited production rate and another problem is its mechanical strength limitations which could be a concern for energy storage where structural integrity is required.[28] The PVDF-HFP copolymer has received great attention as a polymer host GPE.[29,30] Though, there are very few reports on PVDF-HFP as a polymer host synthesized by solution casting technique for room temperature NaSBs applications. Especially, there is no report on how different compositions of organic electrolytes affect the conductivity and the performance of room temperature sodium sulfur batteries.

In the present work, we have prepared PVDF-HFP based GPE by a solution casting technique. The ionic conductivities with different compositions of organic electrolytes were investigated. The GPE consists of 1M sodium perchlorate ($NaClO_4$) in propylene carbonate (PC) : ethylene carbonate (EC) (4:1 volume ratio) showed the highest ionic conductivity of 1.37 mS cm^{-1} with wide potential operation stability window of 4.5 V vs Na^+/Na. Electrochemical characterization tests, including cyclic voltammetry and galvanic charge-discharge cycles, were conducted using assembled full cells. Notably, symmetric sodium cells underwent a stripping and plating test that continued uninterrupted for 3000 hours. This impressive performance indicates significant proficiency for developing sustainable sodium-sulfur batteries that offer high energy density and enhanced safety features.

2. Experimental section

2.1 Materials

Sodium cube (Na, 99.9%, Sigma-Aldrich), sodium perchlorate ($NaClO_4$, >98.0%, Sigma-Aldrich), propylene carbonate (PC, >99%, Sigma-Aldrich), ethylene carbonate (EC, 98%, Sigma-Aldrich), polyvinylidene fluoride-co-hexafluoropropylene (PVDF-HFP, average M_W 400,000, pellets, Sigma-Aldrich), and N-Methyl-2-pyrrolidone (NMP, 99.9%, MSE Supplies) are stored in the Ar-filled glovebox (Vacuum Technology Inc, O_2 and H_2O <0.01ppm).

2.2 Material synthesis

2.2.1 Preparation for GPE membrane The LEs were prepared by dissolving 1M $NaClO_4$ in PC:EC (x:1 volume ratio, where x = 1 and 4) and 1M $NaClO_4$ in PC under stirring overnight and the obtained LEs will be denoted as LE11, LE41 and LEPC.–First, gel polymer precursors were prepared by dissolving polyvinylidene fluoride (PVDF, average M_W 534,000, powder, Sigma-Aldrich) in NMP with 1:4 weight ratio overnight. Then, the gel polymer precursors will be stirred with different LEs at 1:1 weight ratio at 50°C overnight and will become GPEs precursors.

. After that, GPEs precursors were cast at 80 μm thickness on 50°C preheated glass plate using doctor blade and will be dried at 50 °C for 12 hours under vacuum environment. The dried GPE was cut into ¾ inch diameter and soaked in the same composition of its LE overnight and will be denoted as GPE11, GPE41 and GPEPC. For example, 0.4g of PVDF-HFP and 1.6g NMP were mixed overnight Then 2g of LE11 was added and stir overnight. After casting, vaccum drying and cutting, the GPE membrane will be immersed in LE11 overnight and become GPE11.

2.2.2 Preparation of sulfur/polyacrylonitrile (SPAN) cathodes SPAN was synthesized following Wei et. al. experiment.[31] In brief, sulfur (S, 99.998%, Sigma-Aldrich) was mixed with polyacrylonitrile (PAN, average M_W 150,000 (typical), Sigma-Aldrich) with 4:1 weight ratio using ball mill machine for 4 hours. The SPAN powder was put in tube furnace and heated at 450°C with 5°C/min ramping rate in Ar flow environment for 6 hours. The baked SPAN was mixed with carbon black (super P, MSE) and 5wt% PVDF in NMP mixture with weight ratio of 8:1:1, respectively, with additional NMP to lessen the viscosity. Next, the prepared compound was mixed by using a vortex mixer and sonicator bath. The as-prepared slurry was cast on carbon-coated aluminum foil (16 μm, MTI Co., USA) with a thickness of 20 μm using doctor blade. The coating was dried overnight at 70°C in vacuum oven. Finally, cathodes 12.7 mm in diameter were punched out and stored in the glovebox. The obtained cathodes have an average sulfur loading of 0.79-1.26 mg cm^{-2}.

3. Characterization

3.1 Physicochemical characterization

Functional group identification and probable inter/intra-molecular interactions are characterized using Fourier transform infrared (FTIR) spectroscopy (The Nicolet 6700 FTIR Spectrometer), in the range of ~4000–400 cm^{-1} by averaging 64 scans with a resolution of ~2 cm^{-1}. Scanning electron microscopy (SEM) was employed (TESCAN VEGA with an accelerating voltage of 2.0 kV) on the dried and soaked GPE41 samples to evaluate morphology. Thermal gravimetric analysis (TGA) was done by TGA 5500 with temperature range from room temperature to 800°C with 5°C/min in N_2 environment. Differential scanning calorimeter (DSC) data were acquired with a Netzsch STA 449 F3 Jupiter TGA/DSC instrument. The sample with ~10-20 mg was cooled to -100°C from its initial temperature and then it was heat from -100°C to 100°C with 5°C/min rate and under N_2 atmosphere.

3.2 Electrochemical characterization

Electrochemical tests were performed in R2032 cells assembled in an Ar-filled glovebox (O_2, H_2O <0.01 ppm). Freshly Na metal cube was cut, pressed and punched into 12.7 mm diameter electrode with thickness of ~0.2mm. A full cell consists of a Na metal anode, GPE and a SPAN cathode. For LE cells, Whatman™ GF/A separators were used and punched into ¾ inch diameter with 80 μL electrolyte of 1M $NaClO_4$ in PC. Cell fabrication was carried out in an argon-filled glovebox and rested for 12 hours before electrochemical characterization. For linear sweep voltammetry (LSV) study, a cell with working electrode as stainless steel and counter electrode /reference electrode as sodium metal will be examined with a scan rate of 0.1mV/s along the voltage window between -0.2-5 V vs Na/Na^+. Potentiostatic electrochemical impedance

spectroscopy (PEIS), were conducted using a Biologic SP-50e integrated frequency response analyzer. PEIS was performed at a constant voltage of 10mV alternating current with frequencies ranging from 800kHz to 100mHz. Cyclic voltammetry (CV) measurements were performed between 0.8-3V, using SPAN as working electrode and sodium as reference and counter electrodes with different scan rates using Biologic MPG-2. Galvanostatic charge/discharge (GCD) and stripping/plating test were performed by NEWARE batteries testing system. Galvanostatic cycling was performed at different C rates (1C = 1675 mAh g_s^{-1}) with voltage window between 0.8-3 V vs Na/Na^+.

Abbreviations

LEs

Liquid electrolytes

PEs

Polymer electrolytes

GPEs

Gel polymer electrolytes

LEPC

1M $NaClO_4$ in PC

LE11

1M $NaClO_4$ in PC:EC (1:1 v/v)

LE41

1M $NaClO_4$ in PC:EC (4:1 v/v)

GPEPC

GPE has LEPC entrapped in PVDF-HFP after vacuum drying and swell after immersing LEPC

GPE11

GPE has LE11 entrapped in PVDF-HFP after vacuum drying and swell after immersing LE11

GPE41

GPE has LE41 entrapped in PVDF-HFP after vacuum drying and swell after immersing in LE41

4. Results and discussion

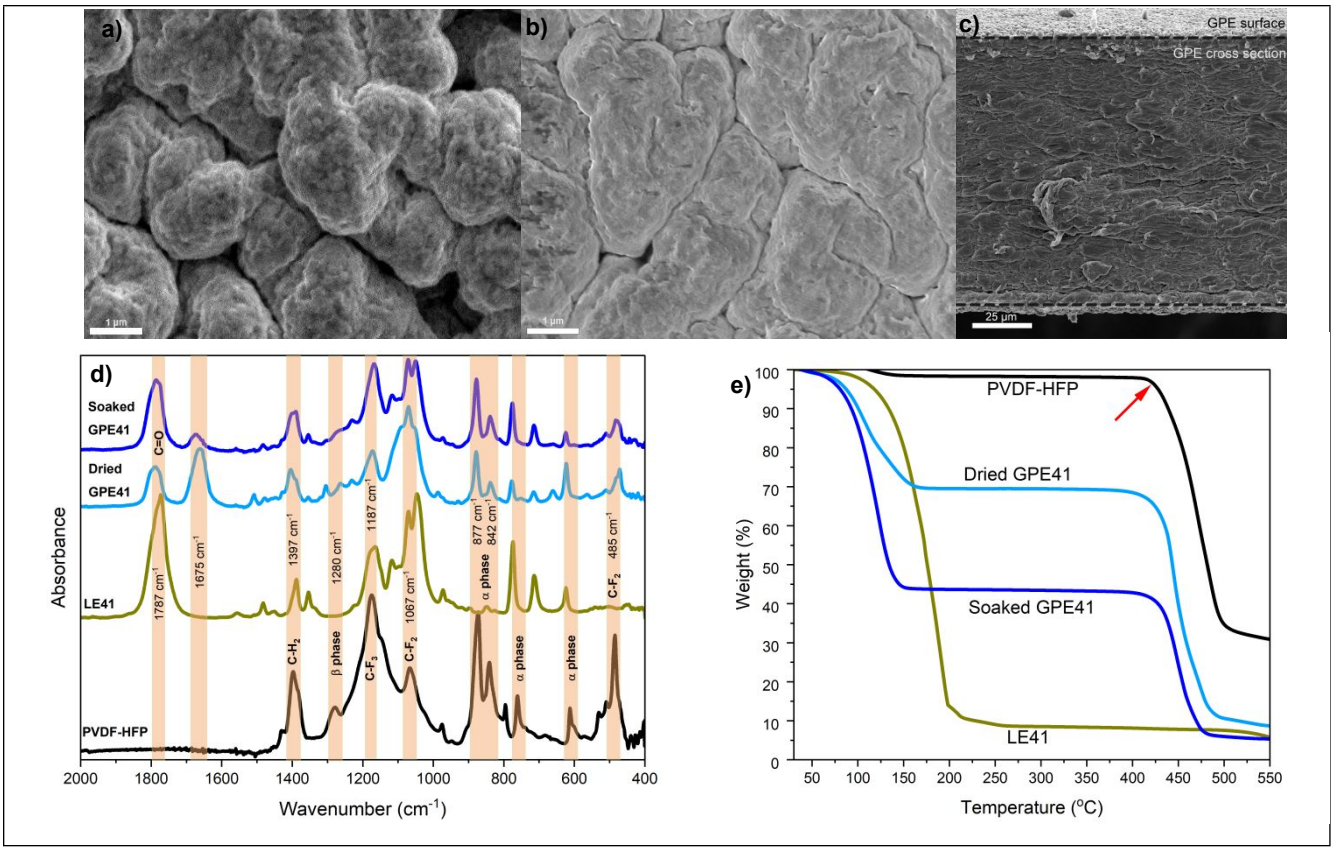

Figure 1. SEM of a) dried GPE41 and b) soaked GPE41. c) SEM image of cross-section of soaked GPE41. d) FTIR of pristine PVDF-HFP, LE41), GPE41 after vacuum-dried and GPE41 after soaking in LE41. e) TGA of pristine PVDF-HFP, dried GPE41, soaked GPE41 and LE41.

The morphology evolution of GPE was systematically investigated using SEM shown in Fig. 1(a-c) and Fig S5. In the dried state (fig 1a and S5a), the GPE membrane exhibited a porous surface morphology with pores diameter of 1-5 µm. This interconnected porous structure facilitates efficient absorption of liquid electrolyte while mitigating leakage risks.[9] Moreover, this porous framework provides sufficient space for the expansion of polymer matrix after LE absorption Following overnight soaking in LE, PVDF-HFP matrix underwent significant swelling (Fig. 1b and S5b), encapsulating the electrolyte within its structure. The expansion of the membrane potentially enhances internal surface contract between polymer chains, thereby promoting ion transport pathways and elevating ionic conductivity. Additionally, the interfacial contact area between electrode/electrolyte also increases with swollen GPE, which is critical for electrochemical performance. Cross-sectional SEM image (Fig 1c) revealed uniform membrane thickness of ~120 µm and the GPE membrane is thinner than the commercialized Whatman™ GF/A separator (260-290 µm). Crucially, the polymer matrix retained structural consistency after both vacuum drying and LE immersion, demonstrating robust mechanical stability and no observable degradation of the PVDF-HFP framework.

FTIR spectroscopy studies (Fig. 1d) were performed to examine the molecular interactions between the liquid electrolyte and the polymer matrix, as well as to analyze the changes in the polymer host due to the entrapment and dispersion of the $NaClO_4$ containing liquid electrolyte.

Figure 1d illustrates the comparative FTIR spectra of pristine PVDF-HFP, LE41, dried GPE41, and soaked GPE41, within the wavenumber range of 400 to 2000 cm^{-1}. Assignment of the important IR bands associated with the host polymer PVDF-HFP, PC, EC, perchlorate (ClO_4^-) anions are given in supporting information, Table S1.

The following distinctive features have been extracted from the spectral response: The peaks at 877 and 842 cm^{-1} present α phase conformation of the semi-crystalline PVDF-HFP.[32–36] The α phase peaks slightly shifts to higher wave number after incorporating LE in polymer matrix.[9] The peaks at 1675 cm^{-1} represent C=O stretching vibration of NMP solvent entrapped in GPE. The peaks at 1397 cm^{-1} and 1187 cm^{-1} shows C-H_2, C-F_3 stretching in PVDF-HFP, respectively.[37–39] The peak 1787 cm^{-1} corresponds to cyclic carbonate in PC and EC which shifts to higher position 1807cm^{-1} in both dried and soaked GPE. This behavior corresponds to the H-C=C-F stretching vibration modes of polyene, suggesting the partial dehydrofluorination of PVDF-HFP chains.[40] NMP solvent functions as a Lewis base, which induces chemical dehydrofluorination of PVDF-HFP skeleton to activate the movements of PVDF-HFP chains, which enhances the interactions among polymer chains.[41] The dehydrofluorination process can enhance the amorphous content of the polymer, potentially resulting in higher LE absorption and improved ionic conductivity of the electrolyte.[42] These observations indicate a complex interplay between the solvent, polymer and electrolyte components, leading to structural modifications that may significantly influence the GPE's electrochemistry properties.

To further examine the material's thermal behavior, thermal gravimetric analysis was used. Fig. 1e shows the thermal gravimetric curves from PVDF-HFP membrane, LE11, dried GPE41 and soaked GPE41. The PVDF-HFP membrane shows thermal stability until 140°C and its initial mass reduction around 170°C is related to the evaporation of NMP components. No weight loss has been observed for PVDF-HFP after 140°C until reaching 420°C where PVDF-HFP decomposition happens. A gradual weight loss of ~5wt% around 100°C for samples dried GPE41 and soaked GPE41 which is possibly attributed to the loss of moisture absorbed by polymer from experiment environment. The substantial weight loss occurred between 120°C-200°C was due to the evaporation of LE in dried GPE41 and soaked GPE41. This weight loss reveals that more than 20wt% of LE41 was incorporated inside the dried GPE41 after the synthesis process. Along with immersing dried membrane GPE41 into LE41 overnight, the GPE41 swelled and became transparent (showed in Fig. S1) increasing the LE content to more than 50wt%. The polymer PVDF-HFP and GPE underwent a second significant mass reduction between 450°C and 500°C, matching with the beginning of its thermal decomposition. During this stage, the PVDF-HFP structure begins to break down thermally, and the backbone of the polymer starts to degrade.[43–45] This stage marks a critical point (indicated by the red arrow in Fig. 1e) in the material's thermal behavior, represents polymer molecular structure deterioration due to the high temperatures.

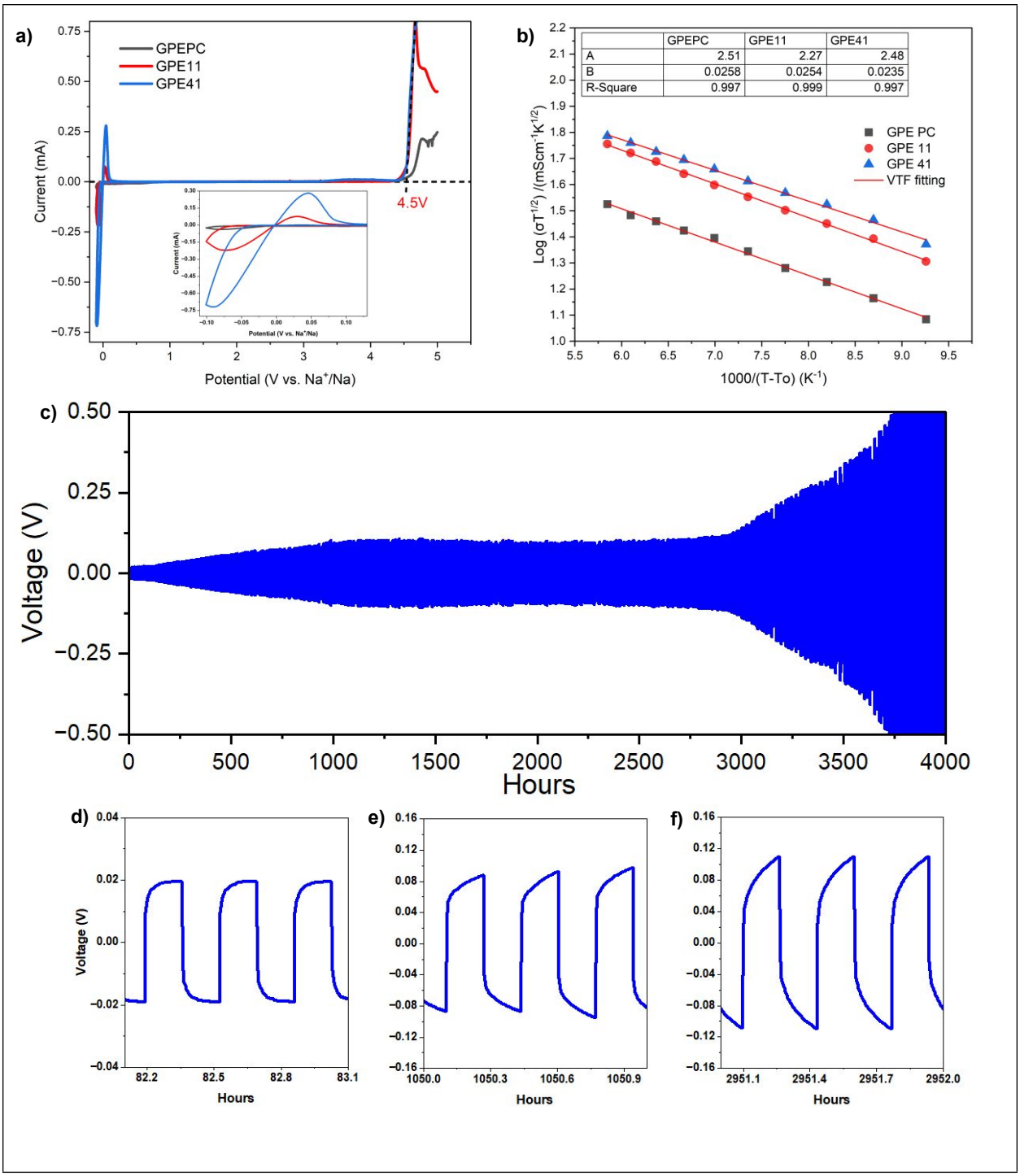

Figure 2. a) LSV of GPE containing various compositions in the voltage range of -0.10V to 5V at a scan rate of 0.1mV s^{-1}. b) VTF fitted plots of ionic conductivity for polymer electrolytes containing various compositions. The inset table in figure 2b summarizes the VTF parameters of B determined from the linear plot log$\sigma T^{1/2}$ versus $1/(T-T_o)$. c) Galvanostatic stripping and plating performance of symmetric cells Na|GPE41|Na with d-f) are zoom in at different time.

The electrochemical stability window or potential window represents a voltage range within which an electrolyte can remain stable without undergoing unwanted side reactions. This crucial

parameter plays a significant role in determining the maximum operating voltage of a battery, directly influencing its energy density and longevity. A wider electrochemical stability window allows for higher operating voltages, potentially enhancing battery performance. To evaluate electrochemical stability window, LSV measurements of GPEs were Fig. 2a illustrates the electrochemical stability windows of GPE PC, GPE11, and GPE41. The graph shows a pair of redox peaks at around 0V, which correspond to the sodium ion plating and stripping on electrodes.[46] The cell ran steadily with no change in current up to 4.5V (vs. Na^+/Na) at ambient temperature which indicates that GPE doesn't have any impurity during fabrication process, and it didn't go under any side reaction with sodium metal. The degradation of GPE membrane is beyond 4.5V which is more than sufficient to operate NaSBs at room temperature. Typically, an GPE that does not undergo a redox reaction under the battery working voltage range (0.8 to 3 V in this work) can be considered as an ideal GPE.[47–49] The wide electrochemical window (0-4.5V) plays an exceedingly important role in the electrochemical stability of NaSBs. As the new energy density and voltage of new generation of batteries increases, the separator film also faces challenges of bearing a high voltage. This wide range of electrochemical potential is more than sufficient to operate not only for NaSBs but also for sodium ion batteries, which makes GPE41 as an ideal electrolyte candidate for both NaSBs and sodium ion batteries.[7,50–53]

Table S2 shows the ionic conductivities of GPE PC, GPE 11 and GPE41 at various temperatures using AC impedance spectroscopy and conductivity equation (1):

$$\sigma = \frac{L}{A\,R_b} \quad (1)$$

Where: L, thickness of membrane. A, area of the membrane. R_b, bulk resistance from the EIS plot.

The GPE membrane was placed between stainless steel surfaces to fabricate SS|GPE|SS coin cells for conductivity measurement. Fig. 2b shows the temperature variations of the conductivity of all the polymer complexes. As temperature increases, the conductivity also increases for all the compositions. The non-linearity in Arrhenius plots indicates that ion transport in polymer electrolytes is dependent on polymer segmental motion. The curvature behavior of the plots suggests that the data can be better described by the Vogel–Tamman–Fulcher (VTF) equation, typical of disordered systems:[54]

$$\sigma = AT^{-1/2} exp\left(\frac{-B}{k_B\,(T - T_o)}\right) (2)$$

where A is a fitting constant proportional to the number of charge carriers, B the pseudo-activation energy associated with the motion of the polymer segment, k_B the Boltzmann constant and T_o is taken as the equilibrium temperature of the system corresponding to zero configuration entropy. T_o is found to be equal to Tg − 50K, where Tg represents the thermodynamic glass transition temperature of the samples (Fig. S6).[55–57] As shown in Fig. 2b, VTF plot was well fitted for all studied GPE (R^2 >0.99). GPE41 had the lowest pseudo-activation energy at 0.0235 eV and highest conductivity at 1.37 mS cm^{-1} at ambient temperature, compared to 0.0254 eV with 1.17 mS cm^{-1} and 0.0258 eV with 0.7 mS cm^{-1} for GPE11 and GPEPC, correspondingly. As temperature rises, polymer chains in electrolytes experience more rapid bond rotations and enhanced segmental

motion. This enhanced molecular mobility creates a more favorable environment for ion transport, facilitating both inter-chain hopping and intra-chain movement of ions.[58] The combined effect improved ion transport mechanisms results in an increase in the overall ionic conductivity of the polymer electrolyte. This temperature-dependent behavior is crucial for understanding and optimizing the performance of polymer electrolytes in various applications. The increased sodium ion mobility leads to improved overall ionic conductivity in the electrolyte. More efficient ion transport can lead to more uniform plating and stripping of sodium at the electrode surfaces, potentially reducing dendrite formation and improving long-term cycling stability.[59,60]To gain insights into plating and stripping behavior of Na, the galvanic test was employed in symmetric Na|GPE41|Na coin cells. The coin cell was applied 0.1 mA cm^{-2} for 15 minutes of charge and 15 minutes of discharge. Fig. 2c shows the coin cell utilized GPE41 went over thousands of cycles and approached 3000 hours of operation before the overpotential significantly increases, which is due to long operation and possibly electrolyte decomposition/aging.[61] There was a slight increase in overpotential from 0.02V(fig. 2d) to 0.1V(fig. 2e) at 0 hour to around 1000 hours. The increased overpotential was contributed by the buildup of stable solid electrolyte interface (SEI) layer. Impressively, from 1000 hours to 3000 hours (fig. 2f), the coin cells function smoothly without any rise in overpotential. Stripping/plating of Na using GPE membrane with difference composition of organic liquid electrolytes (fig. S2) shows that GPE41 has the smallest overpotential compared to GPEPC and GPE11. The best performance in stripping/plating is GPE41 reveals that a higher amount of PC is more compatibility with the battery system. The partial dehydrofuorination process of PVDF backbone where results in formation stable Na-F SEI as it has been reported in previous study.[62,63] The rich Na-F SEI layer not only stabilizes the sodium ion deposition, but also restrains the growth of dendrite effectively.[62,64–68] These contributions enable excellent cycling performance in Na|GPE41|Na for 3000 hours progression. A difference current density study was also applied to sodium symmetric cells utilizing GPE41, shown in Fig. S3. The result indicates that GPE41 can steadily operate from 0.1 to 0.4 mA cm^2 and only failed at 0.5mA cm^2 current density. PVDF-based GPE membrane shows an excellent suppression toward the dendrite formation at electrodes' surface and effective interfacial contact between electrodes/electrolyte. In result, the coin cell was able run for extremely long period without any shortage. Moreover, our result proves that the GPE membrane can function as both separator and ion transport medium with rigid mechanical strength and can tolerate high expansion and contraction of sodium electrode during charge and discharge. The membrane can be utilized for not only sodium sulfur batteries but also sodium ion energy storage.

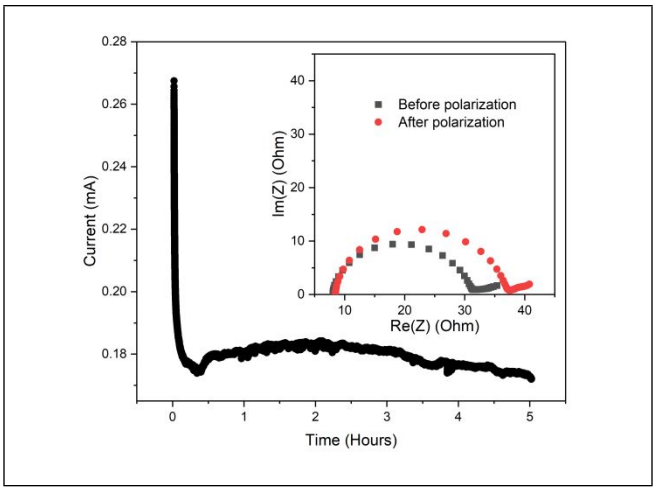

Figure 3: Polarization of Na|GPE41|Na with inset of EIS before and after polarization.

The transference number of Na^+ (t_{Na+}) is a parameter describing Na^+ migration which is crucial in NaSBs. The value of t_{Na} was evaluated using combined AC and DC polarization technique showed in Fig. 3.[69,70] In this technique, the GPE was polarized by applying a small constant voltage of 10mV across the Na|GPE|Na coin cell for 5 hours. Bulk resistances of the cell were measured using electrochemical impedance spectroscopy (EIS) prior and after the polarization process. The t_{Na}^+ of GPE41 is calculated to be 0.648 by using the following equation:

$$t_{Na^+} = \frac{I_s(\Delta V - R_o I_o)}{I_o(\Delta V - R_s I_s)} \quad (3)$$

Where R_o, R_s, I_o, I_s and ΔV are initial resistance, steady state resistance, initial current, steady state current and polarized voltage, respectively. The found t_{Na}^+ of GPE41 is 0.648 and is significantly higher than previous sodium in polymer researches 0.37[51], 0.49[52], respectively.[71–73] In conventional sodium-based electrolytes, because the solvation of Na^+ with the solvent is stronger than the solvation of anions, therefore, the solvent t_{Na}^+ is typically less than 0.5.[74] A higher sodium-ion transport is crucial in NaSBs. This means that a larger fraction of the total current is carried by sodium ions result in minimizing concentration polarization.

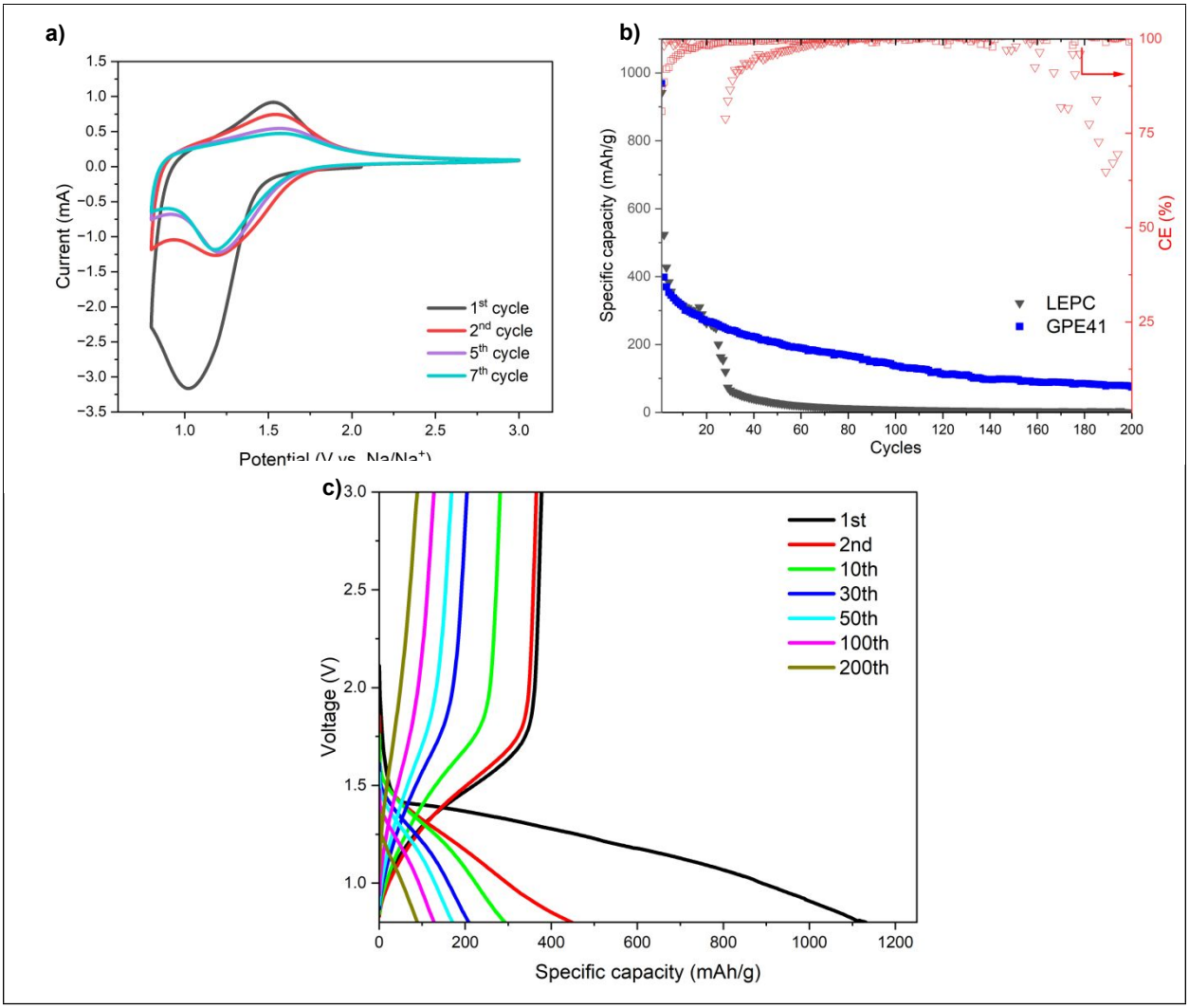

Figure 4: a) cyclic voltammetry of Na|GPE41|SPAN with 0.1 mV s^{-1} scan rate and 0.8V-3V potential window. b) capacity versus cycle from galvanostatic charge & discharge test of full cell Na|GPE41|SPAN at 0.1C. c) voltage profiles of full cell Na|GPE41|SPAN long cycle at 0.1C.

Fig. 4a presents the electrochemical characterization of full cell Na-SPAN The oxidation and reduction potential as well as the reversibility and electrolyte stability of a full cell Na|GPE41|SPAN were conducted from cyclic voltammetry (CV) showed in fig. 4a.[75] Additionally, the CV curves provide insights into the reaction kinetics based on the voltage applied and the corresponding current. The CV curves displayed in Fig. 4a revealing major differences during the redox reaction process at the working electrode surface. During the initial cathodic scan, the current slope starts at around 1.5 V vs. Na/Na^+, corresponding to the solid–liquid transition from sulfur to dissolved Na_2S_x (x = 4-8), and the peak at 1V is related to the formation of solid Na_2S and Na_2S_2, is observed during the first cycle.[49,76] The irreversible peak is characteristic of SPAN cathode.[31] In a subsequent cycle, this discharge peak shifted to 1.2V. The peak shifts during the second cycle go along with a considerable reduction in the polarization of the electrodes during cycling. During discharge, both of the peaks indicates the formation of a mixture of Na_2S_2 and Na_2S.[77] Upon charging, Na_2S is converted into polysulfides (S_x) at 1.7V and all sulfur is bound to

PAN in the fully charged state above 2.28V vs. Na/Na^+.[78,79] After the 2nd cycle, the repetition of CV redox peaks (Fig. 4a) 2nd-7th cycle) confirms that GPE41 membrane act as a functional separator which facilitated the Na-SPAN cells to run multiple cycles.

Long-term galvanostatic cycling of two Na-SPAN cells incorporating GPE41 and LEPC were conducted for 200 cycles. Battery test illustrates the stability of the cells and the high reversibility at 0.1C. GCD shows that the GPE41 cell exhibited the initial specific capacity of ~1000mAh g^{-1} with the reversible capacity was ~398 mAh g^{-1}. With the longevity examination, the LEPC cell failed after 25 cycles whereas GPE still ran steadily to 200 cycles with 99% Coulomb efficiency (CE) and maintained the specific capacity of 74 mAh g^{-1}. With the help of rich Na-F SEI layer from dehydrofuorination of the PVDF-HFP polymer and the incorporation of GPE membrane prevented the short circuit happening in the cells.[42,66,67,80] This synergistic affects allows the batteries to run extensive cycle compared to conventional LE batteries. The results further support the sodium ion uniform deposition using GPE in both full cells and half cells configuration. The comparison of full cells using GPEPC, GPE11 and GPE41 are shown in figure S4 where all of the cells were able to maintain long cycle without short circuit with ~99% CE. Of all, GPE41 provides better compatibility between electrodes electrolyte and was capable of discharge higher 1st and 2nd specific capacity of 1125 and 458 mAh g_{sulfur}^{-1} compared to other cells. Figure 4c is the voltage profile of GPE cell at different cycles. The voltage profile has a consistent charging plateau at around 1.6V which is in agreement with CV results (fig 4a). The voltage profiles do not show any shape change or any additional plateau indicating that GPE matrix does not decompose or have any side reaction after long cycling time.

5. Conclusion

We successfully prepared PVDF-HFP based GPE incorporating $NaClO_4$ and organic electrolyte with different ratio via solution casting technique. A galvanostatic plating and stripping performed on a Na|GPE41|Na cell exhibiting a long-stability lifespan up to 3000 hours of operation without any GPE41 membrane can achieve a high ionic conductivity of 1.37 mS cm^{-1}, high t_{Na^+} ~0.648 at room temperature and the electrochemical stability window of 4.5 V vs Na^+/Na. Na-SPAN cells employed GPE41 electrolyte delivered a discharge capacity of 398 mAh g_{sulfur}^{-1} at 1st reversible cycle and 75mAh g_{sulfur}^{-1} after cycling for 200 cycles with 99% CE. The incorporation of GPEs in Na-SPAN batteries at ambient temperatures presents a promising avenue for advancing Na-Sulfur battery technology. By utilizing GPEs, we anticipate a new paradigm in Na-Sulfur battery development, addressing key challenges and opening up innovative possibilities for high-performance, safer energy storage solutions.

Acknowledgement

This work was supported by the National Science Foundation under Award 2229305.

References

(1) Dunn, B.; Kamath, H.; Tarascon, J.-M. Electrical Energy Storage for the Grid: A Battery of Choices. *Science* **2011**, *334* (6058), 928–935. https://doi.org/10.1126/science.1212741.

(2) Gaines, L. The Future of Automotive Lithium-Ion Battery Recycling: Charting a Sustainable Course. *Sustainable Materials and Technologies* **2014**, *1–2*, 2–7. https://doi.org/10.1016/j.susmat.2014.10.001.

(3) Pigłowska, M.; Kurc, B.; Galiński, M.; Fuć, P.; Kamińska, M.; Szymlet, N.; Daszkiewicz, P. Challenges for Safe Electrolytes Applied in Lithium-Ion Cells—A Review. *Materials* **2021**, *14* (22), 6783. https://doi.org/10.3390/ma14226783.

(4) Wang, Q.; Jiang, L.; Yu, Y.; Sun, J. Progress of Enhancing the Safety of Lithium Ion Battery from the Electrolyte Aspect. *Nano Energy* **2019**, *55*, 93–114. https://doi.org/10.1016/j.nanoen.2018.10.035.

(5) Liu, K.; Liu, Y.; Lin, D.; Pei, A.; Cui, Y. Materials for Lithium-Ion Battery Safety. *Science Advances* **2018**, *4* (6), eaas9820. https://doi.org/10.1126/sciadv.aas9820.

(6) Zhu, Y.; Yang, Y.; Fu, L.; Wu, Y. A Porous Gel-Type Composite Membrane Reinforced by Nonwoven: Promising Polymer Electrolyte with High Performance for Sodium Ion Batteries. *Electrochimica Acta* **2017**, *224*, 405–411. https://doi.org/10.1016/j.electacta.2016.12.030.

(7) Vignarooban, K.; Kushagra, R.; Elango, A.; Badami, P.; Mellander, B.-E.; Xu, X.; Tucker, T. G.; Nam, C.; Kannan, A. M. Current Trends and Future Challenges of Electrolytes for Sodium-Ion Batteries. *International Journal of Hydrogen Energy* **2016**, *41* (4), 2829–2846. https://doi.org/10.1016/j.ijhydene.2015.12.090.

(8) Kang, D.-W.; Kim, J.-K. Characterization of Fibrous Gel Polymer Electrolyte for Lithium Polymer Batteries with Enhanced Electrochemical Properties. *Journal of Electroanalytical Chemistry* **2016**, *775*, 37–42. https://doi.org/10.1016/j.jelechem.2016.05.029.

(9) Kumar, D.; Suleman, Mohd.; Hashmi, S. A. Studies on Poly(Vinylidene Fluoride-Co-Hexafluoropropylene) Based Gel Electrolyte Nanocomposite for Sodium–Sulfur Batteries. *Solid State Ionics* **2011**, *202* (1), 45–53. https://doi.org/10.1016/j.ssi.2011.09.001.

(10) Park, M. J.; Choi, I.; Hong, J.; Kim, O. Polymer Electrolytes Integrated with Ionic Liquids for Future Electrochemical Devices. *Journal of Applied Polymer Science* **2013**, *129* (5), 2363–2376. https://doi.org/10.1002/app.39064.

(11) Kalhoff, J.; Eshetu, G. G.; Bresser, D.; Passerini, S. Safer Electrolytes for Lithium-Ion Batteries: State of the Art and Perspectives. *ChemSusChem* **2015**, *8* (13), 2154–2175. https://doi.org/10.1002/cssc.201500284.

(12) Osada, I.; de Vries, H.; Scrosati, B.; Passerini, S. Ionic-Liquid-Based Polymer Electrolytes for Battery Applications. *Angewandte Chemie International Edition* **2016**, *55* (2), 500–513. https://doi.org/10.1002/anie.201504971.

(13) Tan, S.; Ji, Y. J.; Zhang, Z. R.; Yang, Y. Recent Progress in Research on High-Voltage Electrolytes for Lithium-Ion Batteries. *ChemPhysChem* **2014**, *15* (10), 1956–1969. https://doi.org/10.1002/cphc.201402175.

(14) Kim, J. I.; Choi, Y.; Chung, K. Y.; Park, J. H. A Structurable Gel-Polymer Electrolyte for Sodium Ion Batteries. *Advanced Functional Materials* **2017**, *27* (34), 1701768. https://doi.org/10.1002/adfm.201701768.

(15) Zhu, Y.; Xiao, S.; Shi, Y.; Yang, Y.; Hou, Y.; Wu, Y. A Composite Gel Polymer Electrolyte with High Performance Based on Poly(Vinylidene Fluoride) and Polyborate for Lithium Ion Batteries. *Advanced Energy Materials* **2014**, *4* (1), 1300647. https://doi.org/10.1002/aenm.201300647.

(16) Yang, Y. Q.; Chang, Z.; Li, M. X.; Wang, X. W.; Wu, Y. P. A Sodium Ion Conducting Gel Polymer Electrolyte. *Solid State Ionics* **2015**, *269*, 1–7. https://doi.org/10.1016/j.ssi.2014.11.015.

(17) Nunes-Pereira, J.; Costa, C. M.; Lanceros-Méndez, S. Polymer Composites and Blends for Battery Separators: State of the Art, Challenges and Future Trends. *Journal of Power Sources* **2015**, *281*, 378–398. https://doi.org/10.1016/j.jpowsour.2015.02.010.

(18) Cheng, X.; Pan, J.; Zhao, Y.; Liao, M.; Peng, H. Gel Polymer Electrolytes for Electrochemical Energy Storage. *Advanced Energy Materials* **2018**, *8* (7), 1702184. https://doi.org/10.1002/aenm.201702184.
(19) Muldoon, J.; Bucur, C. B.; Boaretto, N.; Gregory, T.; di Noto, V. Polymers: Opening Doors to Future Batteries. *Polymer Reviews* **2015**, *55* (2), 208–246. https://doi.org/10.1080/15583724.2015.1011966.
(20) Nguyen, H.; Wei, S. Recent Progress of Gel Polymer Electrolytes for Sodium Sulfur Batteries. *ACS Appl. Electron. Mater.* **2024**. https://doi.org/10.1021/acsaelm.3c01841.
(21) Armand, M. B. Polymer Electrolytes. *Annual Review of Materials Science* **1986**, *16* (1), 245–261. https://doi.org/10.1146/annurev.ms.16.080186.001333.
(22) Arya, A.; Sharma, A. L. Polymer Electrolytes for Lithium Ion Batteries: A Critical Study. *Ionics* **2017**, *23* (3), 497–540. https://doi.org/10.1007/s11581-016-1908-6.
(23) Zhou, D.; Shanmukaraj, D.; Tkacheva, A.; Armand, M.; Wang, G. Polymer Electrolytes for Lithium-Based Batteries: Advances and Prospects. *Chem* **2019**, *5* (9), 2326–2352. https://doi.org/10.1016/j.chempr.2019.05.009.
(24) Abbrent, S.; Plestil, J.; Hlavata, D.; Lindgren, J.; Tegenfeldt, J.; Wendsjö, Å. Crystallinity and Morphology of PVdF–HFP-Based Gel Electrolytes. *Polymer* **2001**, *42* (4), 1407–1416. https://doi.org/10.1016/S0032-3861(00)00517-6.
(25) Janakiraman, S.; Padmaraj, O.; Ghosh, S.; Venimadhav, A. A Porous Poly (Vinylidene Fluoride-Co-Hexafluoropropylene) Based Separator-Cum-Gel Polymer Electrolyte for Sodium-Ion Battery. *Journal of Electroanalytical Chemistry* **2018**, *826*, 142–149. https://doi.org/10.1016/j.jelechem.2018.08.032.
(26) Liu, T.; Chang, Z.; Yin, Y.; Chen, K.; Zhang, Y.; Zhang, X. The PVDF-HFP Gel Polymer Electrolyte for Li-O2 Battery. *Solid State Ionics* **2018**, *318*, 88–94. https://doi.org/10.1016/j.ssi.2017.08.001.
(27) Ribeiro, C.; Costa, C. M.; Correia, D. M.; Nunes-Pereira, J.; Oliveira, J.; Martins, P.; Gonçalves, R.; Cardoso, V. F.; Lanceros-Méndez, S. Electroactive Poly(Vinylidene Fluoride)-Based Structures for Advanced Applications. *Nat Protoc* **2018**, *13* (4), 681–704. https://doi.org/10.1038/nprot.2017.157.
(28) Senthilkumar, S. H.; Ramasubramanian, B.; Rao, R. P.; Chellappan, V.; Ramakrishna, S. Advances in Electrospun Materials and Methods for Li-Ion Batteries. *Polymers* **2023**, *15* (7), 1622. https://doi.org/10.3390/polym15071622.
(29) Barbosa, J. C.; Dias, J. P.; Lanceros-Méndez, S.; Costa, C. M. Recent Advances in Poly(Vinylidene Fluoride) and Its Copolymers for Lithium-Ion Battery Separators. *Membranes* **2018**, *8* (3), 45. https://doi.org/10.3390/membranes8030045.
(30) Zhou, L.; Cao, Q.; Jing, B.; Wang, X.; Tang, X.; Wu, N. Study of a Novel Porous Gel Polymer Electrolyte Based on Thermoplastic Polyurethane/Poly(Vinylidene Fluoride-Co-Hexafluoropropylene) by Electrospinning Technique. *Journal of Power Sources* **2014**, *263*, 118–124. https://doi.org/10.1016/j.jpowsour.2014.03.140.
(31) Wei, S.; Ma, L.; Hendrickson, K. E.; Tu, Z.; Archer, L. A. Metal–Sulfur Battery Cathodes Based on PAN–Sulfur Composites. *J. Am. Chem. Soc.* **2015**, *137* (37), 12143–12152. https://doi.org/10.1021/jacs.5b08113.
(32) Pandey, G. P.; Hashmi, S. A. Experimental Investigations of an Ionic-Liquid-Based, Magnesium Ion Conducting, Polymer Gel Electrolyte. *Journal of Power Sources* **2009**, *187* (2), 627–634. https://doi.org/10.1016/j.jpowsour.2008.10.112.
(33) Kumar, D.; Hashmi, S. A. Ionic Liquid Based Sodium Ion Conducting Gel Polymer Electrolytes. *Solid State Ionics* **2010**, *181* (8), 416–423. https://doi.org/10.1016/j.ssi.2010.01.025.
(34) Aravindan, V.; Vickraman, P. Lithium Fluoroalkylphosphate Based Novel Composite Polymer Electrolytes (NCPE) Incorporated with Nanosized SiO2 Filler. *Materials Chemistry and Physics* **2009**, *115* (1), 251–257. https://doi.org/10.1016/j.matchemphys.2008.11.062.
(35) Saikia, D.; Wu, H.-Y.; Pan, Y.-C.; Lin, C.-P.; Huang, K.-P.; Chen, K.-N.; Fey, G. T. K.; Kao, H.-M. Highly Conductive and Electrochemically Stable Plasticized Blend Polymer Electrolytes Based on

PVdF-HFP and Triblock Copolymer PPG-PEG-PPG Diamine for Li-Ion Batteries. *Journal of Power Sources* **2011**, *196* (5), 2826–2834. https://doi.org/10.1016/j.jpowsour.2010.10.096.
(36) Li, Z.; Su, G.; Wang, X.; Gao, D. Micro-Porous P(VDF-HFP)-Based Polymer Electrolyte Filled with Al2O3 Nanoparticles. *Solid State Ionics* **2005**, *176* (23), 1903–1908. https://doi.org/10.1016/j.ssi.2005.05.006.
(37) Zhang, X.; Liu, T.; Zhang, S.; Huang, X.; Xu, B.; Lin, Y.; Xu, B.; Li, L.; Nan, C.-W.; Shen, Y. Synergistic Coupling between Li6.75La3Zr1.75Ta0.25O12 and Poly(Vinylidene Fluoride) Induces High Ionic Conductivity, Mechanical Strength, and Thermal Stability of Solid Composite Electrolytes. *J. Am. Chem. Soc.* **2017**, *139* (39), 13779–13785. https://doi.org/10.1021/jacs.7b06364.
(38) Zhao, Y.; Bai, Y.; Bai, Y.; An, M.; Chen, G.; Li, W.; Li, C.; Zhou, Y. A Rational Design of Solid Polymer Electrolyte with High Salt Concentration for Lithium Battery. *Journal of Power Sources* **2018**, *407*, 23–30. https://doi.org/10.1016/j.jpowsour.2018.10.045.
(39) Wang, B.; Zhang, H. P.; Yang, L. C.; Qu, Q. T.; Wu, Y. P.; Gan, C. L.; Zhou, D. L. Improving Electrochemical Performance of Graphitic Carbon in PC-Based Electrolytes by Using *N*-Vinyl-2-Pyrrolidone as an Additive. *Electrochemistry Communications* **2008**, *10* (10), 1571–1574. https://doi.org/10.1016/j.elecom.2008.08.018.
(40) Farooqui, U. R.; Ahmad, A. L.; Hamid, N. A. Effect of Polyaniline (PANI) on Poly(Vinylidene Fluoride-Co-Hexaflouro Propylene) (PVDF-Co-HFP) Polymer Electrolyte Membrane Prepared by Breath Figure Method. *Polymer Testing* **2017**, *60*, 124–131. https://doi.org/10.1016/j.polymertesting.2017.03.012.
(41) Jie, J.; Liu, Y.; Cong, L.; Zhang, B.; Lu, W.; Zhang, X.; Liu, J.; Xie, H.; Sun, L. High-Performance PVDF-HFP Based Gel Polymer Electrolyte with a Safe Solvent in Li Metal Polymer Battery. *Journal of Energy Chemistry* **2020**, *49*, 80–88. https://doi.org/10.1016/j.jechem.2020.01.019.
(42) Castillo, J.; Robles-Fernandez, A.; Cid, R.; González-Marcos, J. A.; Armand, M.; Carriazo, D.; Zhang, H.; Santiago, A. Dehydrofluorination Process of Poly(Vinylidene Difluoride) PVdF-Based Gel Polymer Electrolytes and Its Effect on Lithium-Sulfur Batteries. *Gels* **2023**, *9* (4), 336. https://doi.org/10.3390/gels9040336.
(43) Mouraliraman, D.; Shaji, N.; Praveen, S.; Nanthagopal, M.; Ho, C. W.; Varun Karthik, M.; Kim, T.; Lee, C. W. Thermally Stable PVDF-HFP-Based Gel Polymer Electrolytes for High-Performance Lithium-Ion Batteries. *Nanomaterials (Basel)* **2022**, *12* (7), 1056. https://doi.org/10.3390/nano12071056.
(44) Peng, G.; Zhao, X.; Zhan, Z.; Ci, S.; Wang, Q.; Liang, Y.; Zhao, M. New Crystal Structure and Discharge Efficiency of Poly(Vinylidene Fluoride-Hexafluoropropylene)/Poly(Methyl Methacrylate) Blend Films. *RSC Adv.* **2014**, *4* (32), 16849–16854. https://doi.org/10.1039/C3RA47462C.
(45) Mahant, Y. P.; Kondawar, S. B.; Nandanwar, D. V.; Koinkar, P. Poly(Methyl Methacrylate) Reinforced Poly(Vinylidene Fluoride) Composites Electrospun Nanofibrous Polymer Electrolytes as Potential Separator for Lithium Ion Batteries. *Mater Renew Sustain Energy* **2018**, *7* (2), 5. https://doi.org/10.1007/s40243-018-0115-y.
(46) Tanwar, M.; Bezabh, H. K.; Basu, S.; Su, W.-N.; Hwang, B.-J. Investigation of Sodium Plating and Stripping on a Bare Current Collector with Different Electrolytes and Cycling Protocols. *ACS Appl. Mater. Interfaces* **2019**, *11* (43), 39746–39756. https://doi.org/10.1021/acsami.9b10097.
(47) Xin, S.; Yin, Y.-X.; Guo, Y.-G.; Wan, L.-J. A High-Energy Room-Temperature Sodium-Sulfur Battery. *Advanced Materials* **2014**, *26* (8), 1261–1265. https://doi.org/10.1002/adma.201304126.
(48) Wei, S.; Xu, S.; Agrawral, A.; Choudhury, S.; Lu, Y.; Tu, Z.; Ma, L.; Archer, L. A. A Stable Room-Temperature Sodium–Sulfur Battery. *Nat Commun* **2016**, *7* (1), 11722. https://doi.org/10.1038/ncomms11722.
(49) Murugan, S.; Niesen, S.; Kappler, J.; Küster, K.; Starke, U.; Buchmeiser, M. R. Ultra-Stable Cycling of High Capacity Room Temperature Sodium-Sulfur Batteries Based on Sulfurated Poly(Acrylonitrile). *Batteries & Supercaps* **2021**, *4* (10), 1636–1646. https://doi.org/10.1002/batt.202100125.

(50) Manthiram, A.; Yu, X. Ambient Temperature Sodium–Sulfur Batteries. *Small* **2015**, *11* (18), 2108–2114. https://doi.org/10.1002/smll.201403257.
(51) Wang, Y.-X.; Zhang, B.; Lai, W.; Xu, Y.; Chou, S.-L.; Liu, H.-K.; Dou, S.-X. Room-Temperature Sodium-Sulfur Batteries: A Comprehensive Review on Research Progress and Cell Chemistry. *Advanced Energy Materials* **2017**, *7* (24), 1602829. https://doi.org/10.1002/aenm.201602829.
(52) Zhao, C.; Liu, L.; Qi, X.; Lu, Y.; Wu, F.; Zhao, J.; Yu, Y.; Hu, Y.-S.; Chen, L. Solid-State Sodium Batteries. *Advanced Energy Materials* **2018**, *8* (17), 1703012. https://doi.org/10.1002/aenm.201703012.
(53) Liu, X.; Jiang, X.; Zeng, Z.; Ai, X.; Yang, H.; Zhong, F.; Xia, Y.; Cao, Y. High Capacity and Cycle-Stable Hard Carbon Anode for Nonflammable Sodium-Ion Batteries. *ACS Appl. Mater. Interfaces* **2018**, *10* (44), 38141–38150. https://doi.org/10.1021/acsami.8b16129.
(54) Baskaran, R.; Selvasekarapandian, S.; Kuwata, N.; Kawamura, J.; Hattori, T. Ac Impedance, DSC and FT-IR Investigations on (*x*)PVAc–(1 − *x*)PVdF Blends with LiClO4. *Materials Chemistry and Physics* **2006**, *98* (1), 55–61. https://doi.org/10.1016/j.matchemphys.2005.08.063.
(55) Dallaev, R.; Pisarenko, T.; Sobola, D.; Orudzhev, F.; Ramazanov, S.; Trčka, T. Brief Review of PVDF Properties and Applications Potential. *Polymers* **2022**, *14* (22), 4793. https://doi.org/10.3390/polym14224793.
(56) Peng, G.; Zhao, X.; Zhan, Z.; Ci, S.; Wang, Q.; Liang, Y.; Zhao, M. New Crystal Structure and Discharge Efficiency of Poly(Vinylidene Fluoride-Hexafluoropropylene)/Poly(Methyl Methacrylate) Blend Films. *RSC Adv.* **2014**, *4* (32), 16849–16854. https://doi.org/10.1039/C3RA47462C.
(57) Voice, A. M.; Southall, J. P.; Rogers, V.; Matthews, K. H.; Davies, G. R.; McIntyre, J. E.; Ward, I. M. Thermoreversible Polymer Gel Electrolytes. *Polymer* **1994**, *35* (16), 3363–3372. https://doi.org/10.1016/0032-3861(94)90896-6.
(58) Subba Reddy, Ch. V.; Sharma, A. K.; Narasimha Rao, V. V. R. Conductivity and Discharge Characteristics of Polyblend (PVP + PVA + KIO3) Electrolyte. *Journal of Power Sources* **2003**, *114* (2), 338–345. https://doi.org/10.1016/S0378-7753(02)00582-7.
(59) Deng, Z.; Mishra, T. P.; Mahayoni, E.; Ma, Q.; Tieu, A. J. K.; Guillon, O.; Chotard, J.-N.; Seznec, V.; Cheetham, A. K.; Masquelier, C.; Gautam, G. S.; Canepa, P. Fundamental Investigations on the Sodium-Ion Transport Properties of Mixed Polyanion Solid-State Battery Electrolytes. *Nat Commun* **2022**, *13* (1), 4470. https://doi.org/10.1038/s41467-022-32190-7.
(60) Karatrantos, A. V.; Khan, S.; Yan, C.; Dieden, R.; Urita, K.; Ohba, T.; Cai, Q. Ion Transport in Organic Electrolyte Solutions for Lithium-Ion Batteries and Beyond. *Journal of Energy and Power Technology* **2021**, *3* (3), 1–36. https://doi.org/10.21926/jept.2103043.
(61) Fang, C.; Tran, T.-N.; Zhao, Y.; Liu, G. Electrolyte Decomposition and Solid Electrolyte Interphase Revealed by Mass Spectrometry. *Electrochimica Acta* **2021**, *399*, 139362. https://doi.org/10.1016/j.electacta.2021.139362.
(62) Muñoz-Márquez, M. A.; Zarrabeitia, M.; Castillo-Martínez, E.; Eguía-Barrio, A.; Rojo, T.; Casas-Cabanas, M. Composition and Evolution of the Solid-Electrolyte Interphase in Na2Ti3O7 Electrodes for Na-Ion Batteries: XPS and Auger Parameter Analysis. *ACS Appl. Mater. Interfaces* **2015**, *7* (14), 7801–7808. https://doi.org/10.1021/acsami.5b01375.
(63) Zhang, X.; Wang, S.; Xue, C.; Xin, C.; Lin, Y.; Shen, Y.; Li, L.; Nan, C.-W. Self-Suppression of Lithium Dendrite in All-Solid-State Lithium Metal Batteries with Poly(Vinylidene Difluoride)-Based Solid Electrolytes. *Advanced Materials* **2019**, *31* (11), 1806082. https://doi.org/10.1002/adma.201806082.
(64) Chen, J.; Liu, T.; Chu, M.; Yu, K.; Xie, X.; Lin, K.; Cheng, Y.; Zhang, X.; Li, J.; Shi, Z. Insight into the Interfacial Reaction Mechanism of FEC and NaF on Na for High Performance Sodium Metal Batteries. *Journal of Materials Chemistry A* **2024**, *12* (37), 25222–25232. https://doi.org/10.1039/D4TA03266G.
(65) Muñoz-Márquez, M. Á.; Zarrabeitia, M.; Passerini, S.; Rojo, T. Structure, Composition, Transport Properties, and Electrochemical Performance of the Electrode-Electrolyte Interphase in Non-

Aqueous Na-Ion Batteries. *Advanced Materials Interfaces* **2022**, *9* (8), 2101773. https://doi.org/10.1002/admi.202101773.
(66) Xu, M.; Li, Y.; Ihsan-Ul-Haq, M.; Mubarak, N.; Liu, Z.; Wu, J.; Luo, Z.; Kim, J. K. NaF-Rich Solid Electrolyte Interphase for Dendrite-Free Sodium Metal Batteries. *Energy Storage Materials* **2022**, *44*, 477–486. https://doi.org/10.1016/j.ensm.2021.10.038.
(67) Zhu, C.; Wu, D.; Wang, Z.; Wang, H.; Liu, J.; Guo, K.; Liu, Q.; Ma, J. Optimizing NaF-Rich Solid Electrolyte Interphase for Stabilizing Sodium Metal Batteries by Electrolyte Additive. *Advanced Functional Materials* **2024**, *34* (5), 2214195. https://doi.org/10.1002/adfm.202214195.
(68) Kubota, K.; Komaba, S. Review—Practical Issues and Future Perspective for Na-Ion Batteries. *J. Electrochem. Soc.* **2015**, *162* (14), A2538. https://doi.org/10.1149/2.0151514jes.
(69) Wagner, J. B.; Wagner, C. Electrical Conductivity Measurements on Cuprous Halides. *The Journal of Chemical Physics* **1957**, *26* (6), 1597–1601. https://doi.org/10.1063/1.1743590.
(70) Evans, J.; Vincent, C. A.; Bruce, P. G. Electrochemical Measurement of Transference Numbers in Polymer Electrolytes. *Polymer* **1987**, *28* (13), 2324–2328. https://doi.org/10.1016/0032-3861(87)90394-6.
(71) Lei, D.; He, Y.-B.; Huang, H.; Yuan, Y.; Zhong, G.; Zhao, Q.; Hao, X.; Zhang, D.; Lai, C.; Zhang, S.; Ma, J.; Wei, Y.; Yu, Q.; Lv, W.; Yu, Y.; Li, B.; Yang, Q.-H.; Yang, Y.; Lu, J.; Kang, F. Cross-Linked Beta Alumina Nanowires with Compact Gel Polymer Electrolyte Coating for Ultra-Stable Sodium Metal Battery. *Nat Commun* **2019**, *10* (1), 4244. https://doi.org/10.1038/s41467-019-11960-w.
(72) Lu, Y.; Li, L.; Zhang, Q.; Cai, Y.; Ni, Y.; Chen, J. High-Performance All-Solid-State Electrolyte for Sodium Batteries Enabled by the Interaction between the Anion in Salt and Na 3 SbS 4. *Chemical Science* **2022**, *13* (12), 3416–3423. https://doi.org/10.1039/D1SC06745A.
(73) Ma, Q.; Liu, J.; Qi, X.; Rong, X.; Shao, Y.; Feng, W.; Nie, J.; Hu, Y.-S.; Li, H.; Huang, X.; Chen, L.; Zhou, Z. A New Na[(FSO2)(n-C4F9SO2)N]-Based Polymer Electrolyte for Solid-State Sodium Batteries. *J. Mater. Chem. A* **2017**, *5* (17), 7738–7743. https://doi.org/10.1039/C7TA01820G.
(74) Huang, F.; Xu, P.; Fang, G.; Liang, S. In-Depth Understanding of Interfacial Na+ Behaviors in Sodium Metal Anode: Migration, Desolvation, and Deposition. *Advanced Materials* **2024**, *36* (41), 2405310. https://doi.org/10.1002/adma.202405310.
(75) Huang, X.; Wang, Z.; Knibbe, R.; Luo, B.; Ahad, S. A.; Sun, D.; Wang, L. Cyclic Voltammetry in Lithium–Sulfur Batteries—Challenges and Opportunities. *Energy Technology* **2019**, *7* (8), 1801001. https://doi.org/10.1002/ente.201801001.
(76) Xu, X.; Zhou, D.; Qin, X.; Lin, K.; Kang, F.; Li, B.; Shanmukaraj, D.; Rojo, T.; Armand, M.; Wang, G. A Room-Temperature Sodium–Sulfur Battery with High Capacity and Stable Cycling Performance. *Nat Commun* **2018**, *9* (1), 3870. https://doi.org/10.1038/s41467-018-06443-3.
(77) Ma, S.; Zuo, P.; Zhang, H.; Yu, Z.; Cui, C.; He, M.; Yin, G. Iodine-Doped Sulfurized Polyacrylonitrile with Enhanced Electrochemical Performance for Room-Temperature Sodium/Potassium Sulfur Batteries. *Chemical Communications* **2019**, *55* (36), 5267–5270. https://doi.org/10.1039/C9CC01612K.
(78) Sheng Eng, A. Y.; Nguyen, D.-T.; Kumar, V.; Sandhya Subramanian, G.; Ng, M.-F.; Wei Seh, Z. Tailoring Binder–Cathode Interactions for Long-Life Room-Temperature Sodium–Sulfur Batteries. *Journal of Materials Chemistry A* **2020**, *8* (43), 22983–22997. https://doi.org/10.1039/D0TA07681C.
(79) Zhang, S. S. Understanding of Sulfurized Polyacrylonitrile for Superior Performance Lithium/Sulfur Battery. *Energies* **2014**, *7* (7), 4588–4600. https://doi.org/10.3390/en7074588.
(80) Zhang, P.; Li, R.; Huang, J.; Liu, B.; Zhou, M.; Wen, B.; Xia, Y.; Okada, S. Flexible Poly(Vinylidene Fluoride-Co-Hexafluoropropylene)-Based Gel Polymer Electrolyte for High-Performance Lithium-Ion Batteries. *RSC Adv.* **2021**, *11* (20), 11943–11951. https://doi.org/10.1039/D1RA01250A.

Data Availability Statement

The data generated and/or analyzed during the current study are available from the corresponding author on reasonable request. Supplementary data that support the findings of this study are openly available.